

Analytic Expressions for the Surface Brightness Profile of GRB Afterglow Images

Jonathan Granot

Centre for Astrophysics Research, University of Hertfordshire, College Lane, Hatfield, Herts, AL10 9AB, UK; j.granot@herts.ac.uk

6 November 2018

ABSTRACT

The exact profile of a gamma-ray burst (GRB) afterglow image on the plane of the sky can provide important constraints on the underlying physics. In particular, it can test whether the magnetic field in the emitting shocked external medium decreases significantly with the distance behind the shock front, or remains roughly constant. Moreover, it enables more accurate measurements of the afterglow image size and the expected scintillation properties. In this work analytic expressions are derived for the afterglow image in power law segments (PLSs) of the afterglow synchrotron spectrum in which the emission originates from a very thin layer just behind the shock, while simple semi-analytic expressions are derived for the remaining PLSs in which the emission arises from the bulk of the shocked fluid. In all cases the expressions are for a general power law external density profile, and are convenient to use in afterglow studies.

Key words: gamma-rays: bursts – radiation mechanisms: nonthermal – shock waves – relativity

1 INTRODUCTION

The direct measurement of the size of the gamma-ray burst (GRB) afterglow image in the radio, both through the quenching of diffractive scintillation (Frail et al. 1997) and more directly using the VLBA (Taylor et al. 2004, 2005; Pihlström et al. 2007), provided good support for the basic dynamical picture of standard afterglow theory (Waxman, Kulkarni & Frail 1998; Oren, Nakar & Piran 2004; Granot, Ramirez-Ruiz & Loeb 2005). The surface brightness profile within the afterglow image can provide additional constraints on the afterglow physics. It can potentially be tested directly for a particularly nearby and reasonably bright GRB afterglow, or even for more distant events in the case of microlensing (Garnavich, Loeb & Stanek 2000; Gaudi, Granot & Loeb 2001, e.g.). In particular, the exact appearance of the afterglow image on the plane of the sky can be very useful in improving the accuracy of the afterglow image size measurements, both when the image is directly but only marginally resolved and its size is determined through fits to the visibility data, and through the quenching of scintillation. It can also improve the estimates for the expected amplitude of scintillation, and thus help in the afterglow modeling.

The dynamics of GRB afterglows before the jet break time, t_{jet} , are well described by the Blandford & McKee (1976, hereafter BM76) self-similar solution, while at later times the exact dynamics of the GRB jet are much

less certain and robust. For this reason, most calculations of the afterglow image so far (Waxman 1997; Sari 1998; Panaitescu & Mészáros 1998; Granot, Piran & Sari 1999a,b; Granot & Loeb 2001) have been for the (quasi-) spherical stage, corresponding to $t < t_{\text{jet}}$ (see, however, Ioka & Nakamura 2001). We shall also address the (quasi-) spherical stage, for the same reasons. In previous works the expressions for the afterglow image are either not very accurate due to some simplifying assumption, or not fully analytic, which makes them inconvenient for others to use. Therefore, in § 2 we derive analytic (§§ 2.1, 2.2) or semi-analytic (§ 2.3) expressions for the surface brightness distribution within the afterglow image, for a general power law external density, and for all of the power law segments (PLSs) of the afterglow synchrotron spectrum that are described in Granot & Sari (2002, hereafter GS02), using the notations of GS02. The magnetic field is assumed to be tangled on small scales with an isotropic distribution in the co-moving frame of the emitting shocked fluid, and hold a constant fraction of the internal energy everywhere. The main results are shown in Figures 1 and 2.

2 DERIVING ANALYTIC EXPRESSIONS FOR THE AFTERGLOW IMAGE

Consider a spherical relativistic blast wave. A photon that is emitted from the shock front at a lab frame time t when the shock radius is R and from an angle θ relative to the line

of sight to the central source (that is located at the origin) reaches the observer at an observed time

$$t_{\text{obs}} = t - \frac{R}{c} \cos \theta, \quad (1)$$

where $t_{\text{obs}} = 0$ corresponds to a photon emitted at the origin (i.e. the central source) at $t = 0$ [i.e. the time when the outflow was launched, $R(t = 0) = 0$]. For convenience we normalize the shock radius by its maximal value along the equal arrival time surface of photons to the observer (along the line of sight, at $\theta = 0$), $y \equiv R/R_l$. For a power law external density profile, $\rho_{\text{ext}} = Ar^{-k}$ with $k < 4$, the Lorentz factor of the shock front during the relativistic phase ($\Gamma \gg 1$) scales as $\Gamma \propto R^{(k-3)/2}$ (BM76), i.e. $\Gamma = \Gamma_l y^{(k-3)/2}$. This implies

$$t - \frac{R}{c} = \int_0^t (1-\beta) dt \approx \int_0^R \frac{dR}{2c\Gamma^2} = \frac{R_l y^{4-k}}{2(4-k)\Gamma_l^2 c} = t_{\text{obs}} y^{4-k}, \quad (2)$$

and that $R_l = 2(4-k)\Gamma_l^2 c t_{\text{obs}} = 4(4-k)\gamma_l^2 c t_{\text{obs}}$, where $\gamma_l = \Gamma_l/\sqrt{2}$ is the Lorentz factor of the fluid just behind the shock at $R = R_l$. Since we are interested in the relativistic regime ($\Gamma \gg 1$), this implies that all the relevant emission is from small angles ($\theta \ll 1$) so we can approximate $\cos \theta \approx 1 - \theta^2/2$, and equations 1 and 2 imply

$$\Gamma_l^2 \theta^2 \approx \frac{1 - y^{4-k}}{(4-k)y}. \quad (3)$$

The distance from the center of the image is given by

$$R_{\perp} = R \sin \theta \approx \frac{R_l}{\sqrt{4-k}\Gamma_l} \sqrt{y - y^{5-k}}, \quad (4)$$

and its maximal value is

$$R_{\perp, \text{max}} = \frac{R_l}{\Gamma_l} (5-k)^{-(5-k)/2(4-k)}, \quad (5)$$

and is obtained at $y_* = R_*/R_l = (5-k)^{-1/(4-k)}$ and $\theta_* = \Gamma_*^{-1} = \Gamma_l^{-1} (5-k)^{-(3-k)/2(4-k)}$, where $\Gamma_* = \Gamma(R_*)$. Therefore, the normalized distance from the center of the circularly symmetric afterglow image is given by

$$x \equiv \frac{R_{\perp}}{R_{\perp, \text{max}}} = \frac{(5-k)^{(5-k)/2(4-k)}}{\sqrt{4-k}} \sqrt{y - y^{5-k}}. \quad (6)$$

2.1 Self-Absorbed Spectral Power Law Segments

Below the self-absorption frequency ν_{sa} (PLSs A, B, C in GS02) the specific intensity (i.e. surface brightness) I_{ν} is equal to the source function ($S_{\nu} = j_{\nu}/\alpha_{\nu}$) at the front end of the equal arrival time surface, $(5-k)^{-1/(4-k)} \leq y \leq 1$ ($R_* \leq R \leq R_l$), where $y = (5-k)^{-1/(4-k)}$ ($R = R_*$) and $y = 1$ ($R = R_l$) correspond to $x = 1$ and $x = 0$, respectively:

$$I_{\nu} = \delta^3 I'_{\nu} = \delta^{3-b} I'_{\nu} = \delta^{3-b} \frac{2\nu^2}{c^2} kT_{\text{eff}}(\nu), \quad (7)$$

where $I'_{\nu} \propto (\nu')^b$, $kT_{\text{eff}}(\nu)$ is the effective temperature of the electrons that radiate in the local rest frame of the emitting fluid just behind the shock at the observed frequency ν , and

$$\delta \equiv \frac{\nu}{\nu'} \approx \frac{2\gamma}{1 + \gamma^2 \theta^2} \approx \frac{2^{3/2}(4-k)\Gamma_l y^{(5-k)/2}}{(7-2k)y^{4-k} + 1}, \quad (8)$$

is the Doppler factor. Primed and un-primed quantities are measured in the comoving (emitting fluid) and lab (or observer) frames, respectively. In PLS A ($\nu_m <$

$\nu < \nu_{\text{sa}}$), $kT_{\text{eff}}(\nu) \approx \gamma_e m_e c^2$ for γ_e that satisfies $\nu \approx \nu'_{\text{syn}}(\gamma_e) \approx eB'\gamma_e^2/(2\pi m_e c)$, so that $kT_{\text{eff}} \propto (\nu/B')^{1/2} \propto \nu^{1/2} \Gamma^{-1/2} \rho_{\text{ext}}^{-1/4} \propto \nu^{1/2} y^{3/4}$ [since $(B')^2 \propto e'_{\text{int}} \propto \rho_{\text{ext}} \Gamma^2$] and $b = 5/2$. Thus

$$I_{\nu} \propto \nu^{5/2} y^{k/4} \left[1 + \frac{1 - y^{4-k}}{2(4-k)y^{4-k}} \right]^{-1/2}, \quad (9)$$

$$\frac{I_{\nu}(x=1)}{I_{\nu}(x=0)} = \sqrt{\frac{2}{3}} (5-k)^{\frac{3-k}{4(4-k)}} \approx \begin{cases} 0.8165 & (k=0), \\ 0.6204 & (k=2). \end{cases}$$

In PLS B ($\nu < \min[\nu_m, \nu_{\text{sa}}, \nu_{\text{ac}}]$), $kT_{\text{eff}} \approx \gamma_m m_e c^2 \propto \Gamma \propto y^{(k-3)/2}$, and therefore $b = 2$ and

$$I_{\nu} \propto \nu^2 \left[y^{3-k} + \frac{1 - y^{4-k}}{2(4-k)y} \right]^{-1}, \quad (10)$$

$$\frac{I_{\nu}(x=1)}{I_{\nu}(x=0)} = \frac{2}{3} (5-k)^{\frac{3-k}{4-k}} \approx \begin{cases} 2.2291 & (k=0), \\ 1.1547 & (k=2). \end{cases}$$

In PLS C ($\nu_{\text{ac}} < \nu < \nu_{\text{sa}}$) the emission is from electrons that have suffered significant cooling. Locally, the electron distribution in this region is approximately mono-energetic, and the electron Lorentz factor scales as $\gamma_e \propto 1/[(B')^2 l']$ with the distance l' behind the shock front (at the comoving time of emission) in the comoving frame (Granot, Piran & Sari 2000). Most of the photons that reach the observer near an observed frequency ν originate near $l'_1(\nu, \mu')$ which is given by $\tau_{\nu}[l'_1(\nu, \mu')] = 1$, where $\mu' = \cos \theta'$, and θ' is the angle between the direction of the photon and the shock normal (i.e. the radial direction) in the comoving frame. Therefore, $kT_{\text{eff}}(\nu) \approx \gamma_e [l'_1(\nu, \mu')] m_e c^2$. The path length of a photon until it overtakes the shock front (which is receding from the shocked fluid at a velocity of $\beta'_{\text{sh}} c \approx c/3$), s' , is related to its initial distance from the shock front, l' , by

$$f \equiv \frac{s'}{l'} = \frac{1}{\mu' - \beta'_{\text{sh}}} \approx \frac{3(1 + \gamma^2 \theta^2)}{2(1 - 2\gamma^2 \theta^2)} \approx \frac{3}{4} \left[\frac{(7-2k)y^{4-k} + 1}{(5-k)y^{4-k} - 1} \right], \quad (11)$$

$$\mu' = \frac{\mu - \beta}{1 - \beta\mu} \approx \frac{1 - \gamma^2 \theta^2}{1 + \gamma^2 \theta^2}.$$

The location of l'_1 is where the optically thin and optically thick fluxes are equal,

$$n' s' (l'_1) \frac{P'_{\nu', \text{max}}}{4\pi} \left(\frac{\nu'}{\nu'_{\text{syn}}[\gamma_e(l'_1)]} \right)^{1/3} = \frac{2(\nu')^2}{c^2} \gamma_e(l'_1) m_e c^2, \quad (12)$$

where $P'_{\nu', \text{max}} \propto B' \propto R^{-3/2}$, $\nu'_{\text{syn}} \propto B' \gamma_e^2 \propto R^{-3/2} \gamma_e^2$, $n' \propto \Gamma \rho_{\text{ext}} \propto R^{-(3+k)/2}$, and $\gamma_e(l'_1) \propto 1/[(B')^2 l'_1]$. In order to use eq. (7) we evaluate eq. (12) at $\nu' = \nu$, so that $l'_1(\nu, \mu') \propto \nu^{5/8} f^{-3/8} (n')^{-3/8} (B')^{-3/2}$ and $kT_{\text{eff}}(\nu) \propto \gamma_e [l'_1(\nu)] \propto f^{3/8} \nu^{-5/8} (n')^{3/8} (B')^{-1/2} \propto \nu^{-5/8} f^{3/8} y^{(3-3k)/16}$, implying $b = 11/8$ and

$$I_{\nu} \propto \nu^{11/8} y^{(5k-18)/8} \left[1 + \frac{1 - y^{4-k}}{2(4-k)y^{4-k}} \right]^{-13/8} \times \left[\frac{(7-2k)y^{4-k} + 1}{(5-k)y^{4-k} - 1} \right]^{3/8}. \quad (13)$$

Note that the surface brightness diverges at the outer edge of the image ($x = 1$), as $I_{\nu} \propto (1-x)^{-3/16}$ for $1-x \ll 1$.

2.2 Fast Cooling Spectral Power Law Segments

For PLSs F ($\max[\nu_c, \nu_{sa}] < \nu < \nu_m$) and H ($\nu > \max[\nu_m, \nu_c, \nu_{sa}]$) the emission comes from electrons that cool on a time-scale much smaller than the dynamical time, and therefore it originates from a very thin layer just behind the shock so we can use the values of γ , n' and B' just behind the shock. We have

$$I_\nu = \delta^3 I'_{\nu'} = \delta^{3-b} I'_{\nu'}, \quad I'_{\nu'} \sim s' j'_{\nu'} \sim f l'_c [\gamma_e(\nu')] j'_{\nu'}, \quad (14)$$

where f is given by eq. (11)¹, $l'_c(\gamma_e) \approx 2\pi m_e^2 / [\sigma_T (B')^2 \gamma_e]$ is the electron cooling length, and $\nu' \equiv \nu'_{\text{syn}}[\gamma_e(\nu')] \approx e B' \gamma_e^2(\nu') / (2\pi m_e c)$. Let $L'_{\nu'} \propto R^a (\nu')^b$ be the spectral luminosity (the total emitted energy of the whole shell [i.e. thin emitting layer of shock fluid] per unit time and frequency, assuming a spherical emitting shell), and $P'_{\nu'}$ be the energy emitted per unit time, volume, and frequency (where both are measured in the comoving frame). For PLS F, $a = (5 - 2k)/4$ and $b = -1/2$, while for PLS H, $a = [14 - 9p + 2k(p - 2)]/4$ and $b = -p/2$ (see Table 1 of Granot 2005). For isotropic emission in the comoving frame we have $j'_{\nu'} = P'_{\nu'} / 4\pi$ and therefore $L'_{\nu'} \sim 4\pi R^2 l'_c[\gamma_e(\nu')] P'_{\nu'} \propto R^2 l'_c[\gamma_e(\nu')] j'_{\nu'} \propto R^2 f^{-1} I'_{\nu'}$, where both $P'_{\nu'}$ and $j'_{\nu'}$ are evaluated inside the thin layer of width $l'_c[\gamma_e(\nu')]$ behind the shock front in which the electrons whose synchrotron frequency is ν' have not yet cooled significantly (and $L'_{\nu'}$ is evaluated using the volume of this layer). Therefore we have $I'_{\nu'} \propto f R^{a-2} (\nu')^b$ and $I'_\nu \propto f R^{a-2} \nu^b$ so that

$$I_\nu \propto \frac{\nu^b \delta^{3-b} f}{y^{2-a}} \propto \frac{\nu^b y^{a+[11-3k-b(5-k)]/2}}{|(5-k)y^{4-k} - 1| [(7-2k)y^{4-k} + 1]^{2-b}}. \quad (15)$$

In order to express I_ν as a function of x rather than y we use eq. (6) to obtain $y(x)$. It is important to note that $y(x)$ it is double valued, where the two values correspond to the front ($y_+ \geq y_*$) and back ($y_- \leq y_*$) of the equal arrival time surface (EATS) of photons to the observer. Here $y_-(x) = R_-(x)/R_l$ corresponds to a photon emitted from the back of the ETAS at a relatively small radius, R_- , and a large emission angle, $\theta > 1/\Gamma(R_-)$, which corresponds to an angle $\theta_{\text{sh}} > 90^\circ$ relative to the radial direction in the rest frame of the shock front, and therefore initially lags behind the shock front. Eventually, at some larger radius R_+ , it catches-up with the shock front and starts moving ahead of it. From R_+ onwards its trajectory coincides with that of a photon emitted from the front of the ETAS [$y_+(x) = R_+(x)/R_l$] at the exact place and time when it crossed the shock front, but at an angle $\theta < 1/\Gamma(R_+)$ that corresponds to $\theta_{\text{sh}} > 90^\circ$ so that it never lags behind the shock front (For more details see Fig. 1 of Granot, Cohen-Tanugi & do Couto e Silva 2008, and the related discussion therein). The two values, $y_-(x)$ and $y_+(x)$, coincide at y_* which corresponds to $x = 1$, i.e. at the outer edge of the image, where the surface brightness diverges as $I_\nu \propto (1-x)^{-1/2}$ for $1-x \ll 1$ (Sari 1998; Granot & Loeb 2001). For $k = 3$ the shock Lorentz factor

does not change with radius, the equal arrival time surface becomes an ellipsoid, and there is a particularly simple solution: $y_\pm = \frac{1}{2} (1 \pm \sqrt{1-x^2})$. For the physically interesting case of $k = 2$, which corresponds to the stellar wind of a massive star progenitor, we also obtain an explicit analytic solution:

$$y_\pm(x) = \frac{2}{\sqrt{3}} \cos \left[\frac{1}{3} \left(\pi \mp \arctan \sqrt{x^2 - 1} \right) \right] \quad (\text{for } k = 2). \quad (16)$$

The total value of $I_\nu(x)$ is obtained by summing these two contributions (in § 2.1 only the value corresponding to $y_+ \geq y_*$ should be used, since the back of the EATS is obscured).

For sufficiently large values k [$k > 32/9 \approx 3.556$ for PLS F, and $k > 4(9-p)/(10-p)$ for PLS H] the surface brightness diverges at the center of the image ($x \ll 1$) due to contributions from small radii ($y \ll 1$), as $I_\nu \propto x^{(32-9k)/2}$ for PLS F and as $I_\nu \propto x^{[4(9-p)-(10-p)k]/2}$ for PLS H. Physically the divergence is avoided due to the break down of some underlying assumption, e.g. for $k > 3$ the shock accelerates and was initially non-relativistic at some radius R_{NR} corresponding to $y_{\text{NR}} = R_{\text{NR}}/R_l$ which introduces a cutoff at $x_{\text{NR}} \approx (y_{\text{NR}}/C_k)^{1/2} \ll 1$, where $C_k = (4-k)(5-k)^{-(5-k)/(4-k)}$.

The expression we obtain for $I_\nu(x)$ is slightly different from that obtained by Sari (1998) for $k = 0$. The difference arises since he did not account for the fact that the fluid just behind the shock moves at a different velocity than the shock front itself. We can reproduce his results by replacing f in the expression for I_ν with $1/|\cos \theta_{\text{sh}}|$ where θ_{sh} is the angle between the direction to the observer (i.e. that of the emitted photons that reach the observer) and the shock normal measured in the rest frame of the shock front (which moves at a velocity of $\beta'_{\text{sh}} c \approx c/3$ relative to the comoving rest frame of the shocked fluid), i.e.

$$f \rightarrow \frac{1}{|\cos \theta_{\text{sh}}|} \approx \frac{1 + \Gamma^2 \theta}{|1 - \Gamma^2 \theta^2|} \approx \frac{1 + 2\gamma^2 \theta}{|1 - 2\gamma^2 \theta^2|} \approx \frac{(3-k)y^{4-k} + 1}{|(5-k)y^{4-k} - 1|}. \quad (17)$$

2.3 Spectral Power Law Segments Originating from the Bulk of the Shocked Fluid

In the PLSs that have been treated so far the emission arises from a very thin layer of shocked fluid just behind the shock front. This has enabled the use of the values of the hydrodynamic quantities just behind the shock, and simplified the derivation of the surface brightness distribution within the afterglow image, $I_\nu(x)$, resulting in fully analytic expressions for it. The emission in such PLSs does not depend on the hydrodynamic profile of the shocked fluid downstream of the shock transition, and responds relatively quickly to changes in the external density (although the fact that the contributions to any given observed time are from a wide range of radii still causes significant smoothing of the observed light curve; Nakar & Granot 2007).

Now we turn to calculate $I_\nu(x)$ for PLSs D, G, and E, in which the emission originates from the bulk of the shocked fluid. In these cases one must specify the values of the hydrodynamic quantities everywhere within the region of shocked fluid. For this purpose we use the spherical adiabatic self-similar BM76 solution. In this solution the hydrodynamic variables depend on the self-similar variable χ , and (GS02)

$$x \equiv \frac{R_\perp}{R_{\perp, \text{max}}} = C_k^{-1/2} \sqrt{y - \chi y^{5-k}}, \quad \chi = \frac{y - C_k x^2}{y^{5-k}}, \quad (18)$$

¹ With the exception that here the absolute value of the denominator should be used, as it becomes negative for $y < y_*$ (at the back of the equal arrival time surface) since the photons (initially) move away from the shock in this case.

where $C_k = (4-k)(5-k)^{-(5-k)/(4-k)}$, as well as

$$\gamma = 2^{-1/2} \Gamma_l y^{(k-3)/2} \chi^{-1/2}, \quad (19)$$

$$e' = 2\Gamma_l^2 \rho_{\text{ext}}(R_l) c^2 y^{-3} \chi^{-(17-4k)/[3(4-k)]}, \quad (20)$$

$$n' = 2^{3/2} \Gamma_l n_{\text{ext}}(R_l) y^{-(3+k)/2} \chi^{-(10-3k)/[2(4-k)]}, \quad (21)$$

and

$$\Gamma_l^2 \theta^2 = \frac{1 - \chi y^{4-k}}{(4-k)y}, \quad \gamma^2 \theta^2 = \frac{1 - \chi y^{4-k}}{2(4-k)\chi y^{4-k}},$$

$$\delta \approx \frac{2\gamma}{1 + \gamma^2 \theta^2} \approx \frac{2^{3/2}(4-k)\Gamma_l \chi^{1/2} y^{(5-k)/2}}{(7-2k)\chi y^{4-k} + 1}. \quad (22)$$

Assuming isotropic emission in the comoving frame, $j'_{\nu'} = P'_{\nu'}/4\pi$, and using the fact that $I_\nu = \int j_\nu ds$ where $j_\nu = \delta^2 j'_{\nu'}$, and in our case $ds \approx dR = R_l dy$, one obtains

$$I_\nu(x) = \frac{2(4-k)^2 R_l \Gamma_l^2}{\pi} \int dy \frac{\chi(y,x) y^{5-k} P'_{\nu'}[y, \chi(y,x)]}{[(7-2k)\chi(y,x) y^{4-k} + 1]^2}$$

$$= \frac{2(4-k)^2 R_l \Gamma_l^2}{\pi} \int dy \frac{(y - C_k x^2) y^2 P'_{\nu'}(y,x)}{[(7-2k)(y - C_k x^2) + y]^2}. \quad (23)$$

Now we need to derive $P'_{\nu'}[y, \chi(y,x)]$ and therefore $P'_{\nu'}(y,x)$ for PLSs D, G, and E. For PLSs D ($\nu_{\text{sa}} < \nu < \nu_m < \nu_c$) and G ($\max[\nu_m, \nu_{\text{sa}}] < \nu < \nu_c$), $P'_{\nu'} \sim n' P'_{\nu', \text{max}, e} (\nu'/\nu'_m)^b$ where $P'_{\nu', \text{max}, e} \approx \sigma_T m_e c^2 B'/(3e)$ and $\nu'_m = \nu'_{\text{syn}}(\gamma_m) \approx eB'\gamma_m^2/(2\pi m_e c)$ where $\gamma_m = g\epsilon_e e'/(n' m_e c^2)$ and $g = (p-2)/(p-1)$ for $p > 2$. Thus, for PLSs D where $b = 1/3$ and G where $b = (1-p)/2$ we obtain

$$P'_{\nu'} = \nu'/\delta \propto \nu^b \chi^{[13k-47+b(13+k)]/[6(4-k)]} y^{[b(4-k)-6-k]/2}$$

$$\times \left[(7-2k)\chi y^{4-k} + 1 \right]^b, \quad (24)$$

$$I_\nu \propto \nu^b \int_{y_-(x)}^{y_+(x)} dy \left(\chi^{[7k-23+b(13+k)]/[6(4-k)]} \right)$$

$$\times y^{[b(4-k)+4-3k]/2} \left[(7-2k)\chi y^{4-k} + 1 \right]^{b-2}, \quad (25)$$

where the limits of integration over y are the appropriate roots of the equation $\chi(y,x) = 1$, i.e. $y - y^{5-k} = C_k x^2$ (see subsection 2.2).

For PLS E ($\nu_{\text{sa}} < \nu < \nu_c < \nu_m$), the emission is dominated by regions where all of the electrons have cooled significantly and their energy distribution is practically a delta function, $N(\gamma_e) \approx n'\delta(\gamma_e - \gamma_{\text{max}}(\chi, y))$, where γ_{max} is given by eq. A12 of GS02. Using equations A8 and A9 from that paper, one obtains that for a constant observed time,

$$\gamma_{\text{max}}(\chi, y) \propto \frac{\chi^{(22-5k)/[6(4-k)]} y^{(1+k)/2}}{(\chi^{(19-2k)/[3(4-k)]} - 1)}. \quad (26)$$

Therefore, $P'_{\nu'} \approx n' P'_{\nu', \text{max}, e} (\nu'/\nu'_{\text{max}})^{1/3}$, where $\nu'_{\text{max}} = \nu'_{\text{syn}}(\gamma_{\text{max}}) \approx eB'\gamma_{\text{max}}^2/(2\pi m_e c)$. Altogether, using eq. (23) we obtain

$$I_\nu(x) \propto \nu^{1/3} \int dy \left\{ y^{(4-5k)/3} \left[\frac{\chi^{(19-2k)/[3(4-k)]} - 1}{\chi^{(18-5k)/[2(4-k)]}} \right]^{2/3} \right.$$

$$\left. \times \left[1 + (7-2k)\chi y^{4-k} \right]^{-5/3} \right\}. \quad (27)$$

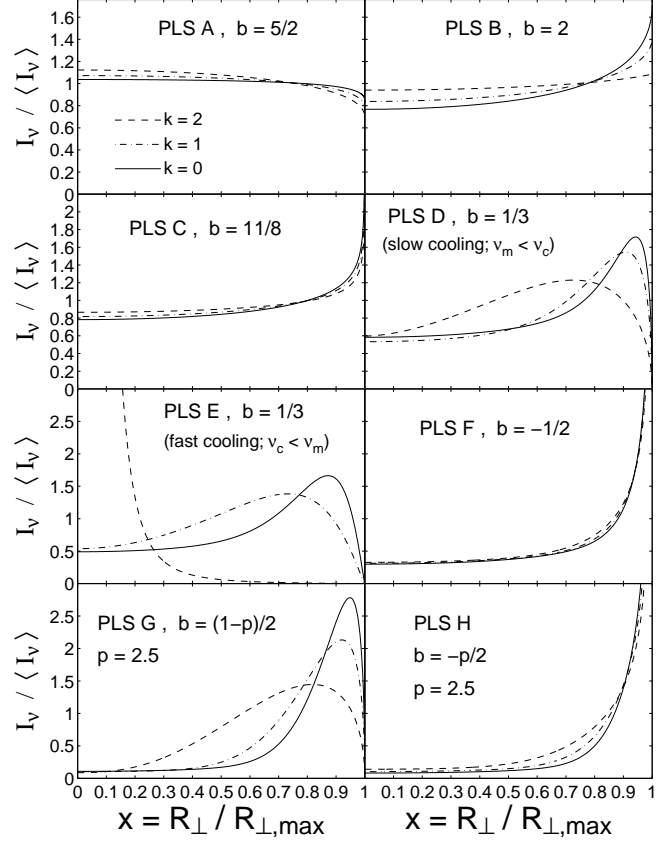


Figure 1. The afterglow images: the surface brightness normalized by its average value as a function of the normalized distance from the center of the image, for all of the different power law segments (PLSs) of the afterglow synchrotron spectrum that are described in GS02, and for three values of the power law index k of the external density, where $\rho_{\text{ext}} \propto r^{-k}$. For PLS E, the normalization of the dashed line for $k = 2$ is arbitrary, since the total flux diverges in that case under our assumptions (see text for details).

It can be shown² that for $k > 37/26 \approx 1.423$, $I_\nu(x \ll 1) \propto x^{2(37-26k)/9}$ so that it diverges at the center of the image, while the flux in this regime is dominated by the contribution from $x \ll 1$ and thus scales as $F_\nu \propto \int_0^1 I_\nu(x) x dx \propto 1/(23-13k)$ for $k < 23/13$ and diverges for $k \geq 23/13 \approx 1.769$. If a lower limit for the range of integration, x_{min} , is introduced then $F_\nu \propto x_{\text{min}}^{4(23-13k)/9}$. Of course, a divergence of the total flux is unphysical, and does not really occur. Instead, the underlying assumptions for this PLS break down in this regime ($k \geq 23/13$), resulting in an introduction of such an $x_{\text{min}} \sim y_{\text{min}}^{1/2}$, and PLS E no longer exists in the same form. A detailed treatment of the interesting behavior in that case is saved for a separate work.

Similarly, in PLS D the surface brightness diverges at the center of the image for $k > 61/26 \approx 2.346$ as $I_\nu(x \ll$

² For $x = 0$ we have $\theta = 0$ and $\chi = y^{k-4}$, and this still approximately holds in the region of interest here ($\chi \sim y^{k-4} \gg 1$, where $\chi y^{4-k} = 1 - C_k x^2/y$ becomes significantly different than 1 only for $y \sim y_{\text{min}} \approx C_k x^2$). Thus $I_\nu \propto \int dy y^{2(14-13k)/9}$ becomes dominated by the lower limit of integration, $y_{\text{min}} \approx C_k x^2$, for $k > 37/26$. In this case $I_\nu \propto y_{\text{min}}^{(37-26k)/9} \propto x^{2(37-26k)/9}$.

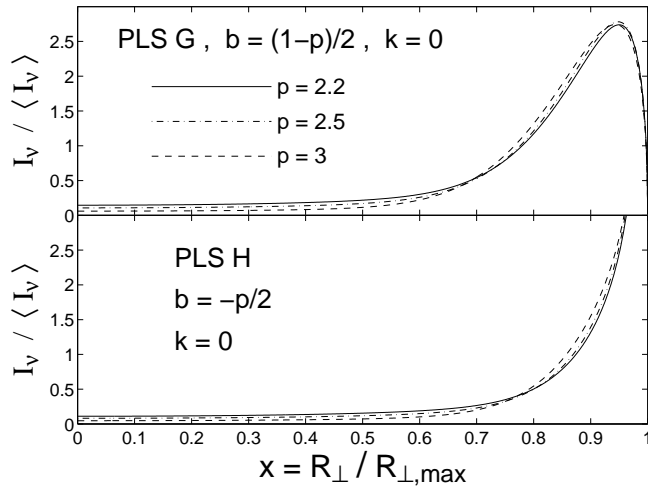


Figure 2. This figure demonstrates the dependence of the afterglow images on the power-law index, p , of the electron energy distribution, in the two PLSs (G and H) where it has some effect. The afterglow image becomes somewhat more limb-brightened as the value of p increases, due to the corresponding decrease in the value of the spectral index b .

1) $\propto x^{2(61-26k)/9}$, and the flux diverges for $k \geq 35/13 \approx 2.692$. In PLS G the surface brightness diverges at the center of the image for³ $k > (32 - 4p)/(11 - p)$ as $I_V(x \ll 1) \propto x^{14-5k-(4-k)(p-1)/2}$, and the flux diverges for $k \geq (36 - 4p)/(11 - p)$. Again, the flux cannot diverge in practice, and this is an indication that the model assumption break down in those regimes.

3 DISCUSSION

Analytic expressions were derived for the afterglow image for PLSs in which the emission originates from a very thin layer just behind the shock (§§ 2.1, 2.2) while simple semi-analytic expressions were obtained for the remaining PLSs in which the emission arises from the bulk of the shocked fluid (§ 2.3). These expressions are for a rather general power law external density profile, $\rho_{\text{ext}} \propto r^{-k}$ with $k < 4$, for which the flow is described by the BM76 self-similar solution. The relevant expressions are given in § 2, and illustrated in Figures 1 and 2. These expressions fully agree with the afterglow images that were shown and used in Granot & Loeb (2001), which were calculated using the formalism of GS02. The flux normalization for the different PLSs, which also provides the surface brightness normalization, can be found in Table 1 of GS02.

The magnetic field in the shocked external medium must be considerably amplified at the shock in order to reproduce the afterglow observations. However, it is not yet clear how far downstream this shock produced magnetic field persists. It could in principle decay considerably at some finite distance behind the shock. If the magnetic field is sig-

nificant only within a thin layer (of width $\Delta \ll R/\gamma^2$) just behind the shock front, and negligible further downstream from the shock (see, e.g. Rossi & Rees 2003), then this will affect the appearance of the afterglow image. In particular, it will affect PLSs where the emission would otherwise originate from the bulk of the shocked fluid (PLSs D, G, and E, which are discussed in § 2.3). In this case, their appearance would resemble those of the fast cooling PLSs, since in both cases the emission arises from a very thin layer just behind the shock, and the image would become extremely limb brightened. This is potentially testable in a microlensing event or if a particularly nearby afterglow image will be well resolved.

Finally, the afterglow image in general depends also on the magnetic field structure (its orientation) in the shocked region, not only on its absolute value (or strength). In this work it was assumed to be tangled on small scales with an isotropic distribution in the comoving frame of the emitting shocked fluid. In this case the emission and absorption coefficients are also isotropic in that frame, which simplifies the calculation of the afterglow image, and it is very useful in this respect. However, such a magnetic field structure predicts no polarization of the afterglow emission, which is inconsistent with the measurement of linear polarization at the level of a few percent that has been detected in the optical or NIR afterglow of several GRBs (see Covino 2004, and references therein). Therefore, in a future work we will discuss the changes that arise for other possible magnetic field structures in the emitting region.

The author gratefully acknowledges a Royal Society Wolfson Research Merit Award.

REFERENCES

- Blandford, R. D., & McKee, C. F. 1976, *Phys. Fluids*, 19, 1130
 Covino, S., et al. 2004, in “Gamma-Ray Bursts in the Afterglow Era” Third Workshop, ed. M. Feroci, F. Frontera, N. Masetti, & L. Piro (San Francisco: ASP), 169
 Frail, D. A., et al. 1997, *Nature*, 389, 261
 Garnavich, P. M., Loeb, A., & Stanek, K. Z. 2000, *ApJ*, 544, L11
 Gaudi, B. S., Granot, J., & Loeb, A. 2001, *ApJ*, 561, 178
 Granot, J. 2005, *ApJ*, 631, 1022
 Granot, J., Cohen-Tanugi, J., & do Couto e Silva, E. 2008, *ApJ*, 677, 92
 Granot, J., & Loeb, A. 2001, *ApJ*, 551, L63
 Granot, J., Piran, T., & Sari, R. 1999a, *ApJ*, 513, 679
 Granot, J., Piran, T., & Sari, R. 1999b, *ApJ*, 527, 236
 Granot, J., Piran, T., & Sari, R. 2000, *ApJ*, 534, L163
 Granot, J., Ramirez-Ruiz, E., & Loeb, A. 2005, *ApJ*, 618, 413
 Granot, J., & Sari, R. 2002, *ApJ*, 568, 820
 Ioka, K., & Nakamura, T. 2001, *ApJ*, 561, 703
 Nakar, E., & Granot, J. 2007, *MNRAS*, 380, 1744
 Oren, Y., Nakar, E., & Piran, T. 2004, *MNRAS*, 353, L35
 Panaitescu, A., & Mészáros, P. 1998, *ApJ*, 493, L31
 Pihlström, Y. M., et al. 2007, *ApJ*, 664, 411
 Rossi, E., & Rees, M. J. 2003, *MNRAS*, 339, 881
 Sari, R. 1998, *ApJ*, 494, L49
 Taylor, G. B., et al. 2004, *ApJ*, 609, L1
 Taylor, G. B., et al. 2005, *ApJ*, 622, 986
 Waxman, E. 1997, *ApJ*, 491, L19
 Waxman, E., Kulkarni, S. R., & Frail, D. A. 1998, *ApJ*, 497, 288

³ This is obtained since for $k(b+1) < -(13b+1)$ the integral in Eq. (25) becomes dominated by a narrow range of y values near the lower limit of integration, where $y \sim y_{\text{min}} \approx C_k x^2$ and $\chi \sim (y - y_{\text{min}})/y_{\text{min}}^{5-k}$ in the range $(C_k x^2)^{5-k} \lesssim y - y_{\text{min}} \lesssim C_k x^2$, and the lower limit of integration dominates.